OPEN ACCESS
Journal of Innovative Optical Health Sciences
Vol. 14, No. 3 (2021) 2150010 (8 pages)

DOI: 10.1142/S1793545821500103



# Model eye tool for retinal optical coherence tomography instrument calibration

Hongting Wang, Wenli Liu, Zhixiong Hu*, Xiuyu Li,
Fei Li and Liangcheng Duan
*Center for Medical Metrology, National Institute of Metrology*
*Beijing 100029, P. R. China*
**huzhixiong@nim.ac.cn*

Received 20 November 2020
Accepted 8 February 2021
Published 7 April 2021

Optical coherence tomography (OCT) has been extensively used as noninvasive tool for biological tissues owing to its three-dimensional imaging ability and high axial resolution. OCT quality assurance is vital in these occasions to keep the reliability and accuracy in medical diagnosis. It is necessary to develop a calibration tool for OCT product manufacture, calibration, and quality control. A practical tool is demanded in the OCT quality control and calibration of OCT. So far, there is no such a practical tool that can test all the key parameters of OCT. We design and fabricate a model eye tool, which has this function. The model eye comprises a doublet lens, a single filament, a piece of glass plate and the microsphere-embedded phantom. The doublets lens is bonded by two pieces of planoconvex lenses in the plane position. The first lens focuses parallel light onto the rear surface of the second lens. The rear surface marked with concentric circles serves as retina to measure the angular field of view (FOV). The small flat surface on the peak of the second lens is used to test signal to noise ratio (SNR). The single filament with 125 $\mu$m diameter is used to check the co-alignment of preview and OCT scan. The empty chamber between the small plane of the second lens and the first surface of glass plate is used to measure the depth scaling of the OCT. The microspheres of 1 $\mu$m diameter distributed uniformly in the phantom, which can test the lateral and the axial resolution of OCT equipment. Experimental results are presented to show the validity of the proposed tool. It is shown that the tool is able to be used in the calibration and quality control of retinal OCT.

*Keywords*: Optical coherence tomography; model eye; microsphere-embedded phantom.

## 1. Introduction

Optical coherence tomography (OCT) is a three-dimensional micro-imaging technique which was firstly proposed by Huang in 1991.[1] OCT has the same level of high resolution as confocal microscopy, but larger imaging depth than confocal microscopy. OCT has the advantage of fast and deep imaging, high resolution and sensitivity, so it is widely used

*Corresponding author.

in medical diagnosis and industrial survey.[2] Owing to its noncontact imaging characteristic, OCT is superior to ultrasound imaging in ophthalmic diagnosis, which can avoid the risk of cross infection.

Ophthalmic OCT is one of the most maturity in terms of OCT application. The ophthalmic OCT was mainly used in the retinal diagnoses, and extended to the area of anterior segment later. In 1991, Huang provided the first demonstration of OCT imaging on human retina.[1] Three years later, Joseph A. Izatt demonstrated the application of OCT to perform imaging in the anterior segment of human eye *in vivo*. Micron-scale resolution measurements of ocular profile, dimensions, and structure in the cornea, anterior angle region, and crystalline lens are reported.[3] The first ophthalmic OCT entered market as diagnostic equipment in 1996, and the first anterior segment OCT (Visante OCT) manufactured by Zeiss showed on the market in 2005. Since then, ophthalmic OCT has been extensively used to measure the physiological parameters of human eye, such as corneal thickness and retinal thickness and to monitor eye disease, e.g., macular edema.[4] The performance of angular field of view (FOV), imaging depth, resolution, imaging speed, and sensitivity has been continually improving.[5] The key parameters of retinal OCT instrument are angular FOV, SNR, co-alignment of preview and OCT scan, depth scaling and resolution. Standard test method and tool have been required for OCT product development, calibration, initial test, and quality control. It is necessary to prove the accuracy of the ophthalmic OCT instrument to ensure its effectiveness in clinical diagnoses. Moreover, it is difficult to acquire consistent data in system validation if human eye works as standard subject. Therefore, a model eye tool that is able to calibrate the key parameters of retina OCT is highly needed.

Several relevant studies were reported in recent years. The National Physical Laboratory (NPL), National Institute of Standards and Technology (NIST), and U.S. Food and Drug Administration (FDA) carried out the researches on the phantom of point spread function (PSF) to measure the OCT resolution.[6–9] Zhixiong Hu made research on PSF phantom and model eye with 3D resolution test targets to evaluate OCT resolution.[10,11] Zhenggang Cao designed model eyes with micro-scale multilayer structure to assess the axial resolution of the OCT.[12] Recently, Baxi has implemented a retinal phantom that emulates the retina with the use of spin coating of nanoparticle-embedded silicone films and laser microetching.[13] Hyun-Ji Lee proposed an advanced retina phantom with a multilayered thin film and microfluidic channels to emulate the human retina so that it can evaluate the quality and accuracy of OCTA images.[14] The OCT resolution can be given by imaging the micro-spheres and calculating the FWHMs based on the PSF theory as mentioned in Refs. 8 and 9. The phantom with micro-spheres were used in our tool to measure the resolution.

The international organization for standardization released an ISO standard (ISO 16971) for the OCT of posterior segment of human eye in 2015,[15] which provided the test method and tool for OCT device. The eye ground of this tool is flat; however, true fundus of true human eye is curved. Hence, the recommended tool is only suitable for small angle in terms of angular FOV. Moreover, the lateral resolution of OCT is not able to be tested using the tool, and the method of SNR measurement is not given by the standard. A practical tool is demanded in the OCT quality control and calibration of OCT. So far, there is no such a practical tool that can test all the key parameters raised by standard ISO 16971.

We develop a model eye tool which can be used to calibrate the key parameters of retinal OCT. The model eye is composed of a doublet lenses (two convex lenses), an angular FOV scale, a single filament, a glass plate, and a microsphere-embedded phantom. The model eye can focus the incident light onto the back surface of itself, which is used to simulate the refractive ability of human eye. The scale on the back of the second lens is applied to test the angular FOV, which is manufactured by laser ablation. The peak of the second lens was cut and a small flat surface is obtained, which is used to test the signal-to-noise ratio (SNR) of OCT. The single filament is used to calibrate the co-alignment of fundus preview and the OCT scan. An empty chamber is formed between the small flat surface and the glass plate. Either the thickness of the chamber or the glass plate can be used to evaluate the depth scaling of the OCT imaging. The empty chamber is the first choice because the empty space is not affected by the accuracy of the refractive index of glass plate. The microsphere-embedded phantom contains microspheres with 1 $\mu$m diameter, which is able to test the lateral and the axial resolution of OCT device. The model eye can work as a practical and useful calibration tool on the

OCT instrument. All the key parameters of OCT can be tested using one model eye, which is cost-effective and convenient.

## 2. Methods

To simulate the optical structure and the refractive power of human eye, we develop the model eye which is shown in Fig. 1. The model eye contains five main parts which are a doublet lenses (two convex lenses), an angular FOV scale, a single filament, a glass plate, and a microsphere-embedded phantom. The free space light going through the first lens can be focused on the back surfaces of the second lens. The scale on the back of the second lens is used to test the angular FOV, which is manufactured by laser ablation. The peak of the second lens was cut and a small flat surface is obtained. The small flat surface is used to test the SNR ratio of OCT. An empty chamber is formed between the small flat surface and the glass plate. Both the thickness of the chamber and the glass plate can be used to evaluate the depth scaling of the OCT imaging. The microsphere-embedded phantom contains microspheres with 1 $\mu$m diameter, which can test the lateral and the axial resolution of OCT device. The single filament is used to calibrate the co-alignment of fundus image and the OCT scan.

The doublet lens contains two convex lenses as shown in Fig. 2. The thickness, curvature radius, and the diameter of the first lens is $h$, $R_1$, and $d$, respectively. The corresponding parameters of the second lens is $H$, $R_2$, and $D$. When $h = R_1$, the axial length of the doublet is expressed as

$$AL_{\mathrm{k}} = R_1 + H. \tag{1}$$

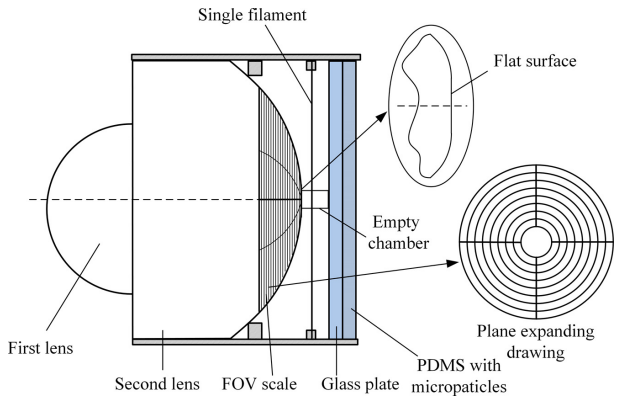


Fig. 1. The structure diagram of the model eye. The angular FOV scale and its expanding drawing is shown.

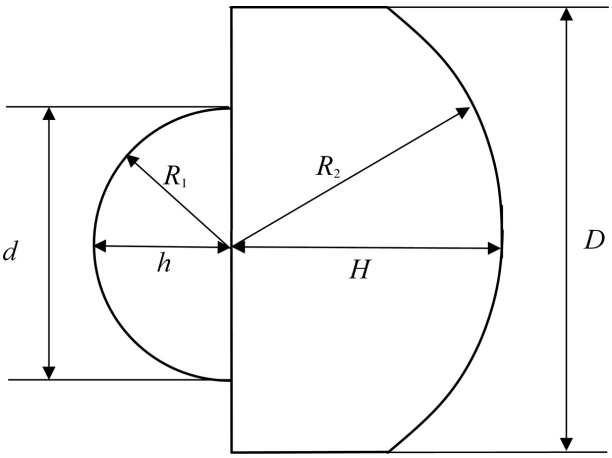


Fig. 2. The doublet lens in the model eye.

Use image formula we have

$$\frac{n}{AL_{\mathrm{k}}} - \frac{1}{S} = \frac{n-1}{R_1}, \tag{2}$$

where $n$ is the refractive index of the two lenses, and $S$ is the distance of far point. The refractive ability of the doublet can be given by $P = 1/S$. The units of $S$ and $P$ are millimeter and meter, respectively. Therefore,

$$P = \frac{1}{S} = 1000\left(\frac{n}{AL_{\mathrm{k}}} - \frac{n-1}{R_1}\right). \tag{3}$$

When refractive diopter is zero, we get

$$AL_{\mathrm{k}} = n \Big/ \frac{n-1}{R_1}. \tag{4}$$

The axial length of the model eye is determined by the refractive index and the curvature radius of the first lens. The focusing property of the model eye depends on $R_1$.

To experimentally demonstrate the proposed tool, we make a model eye and use it to calibrate an OCT device. The K9 doublet lens composes two planoconvex lenses, and they are glued together with decentration $3'$ which is presented in Fig. 3. Set $R_1 = 8$ in Eq. (4), and we get the axial length $AL_{\mathrm{k}} = 23.7\,\mathrm{mm}$. Substitute $AL_{\mathrm{k}} = 23.7\,\mathrm{mm}$ in Eq. (1), and $H = 15.7\,\mathrm{mm}$ is obtained. We make the back surface of the second lens the focal plane, so $R_2 = 15.7\,\mathrm{mm}$. We cut the peak of the second lens with 0.1 mm thickness and obtain a small flat plane.

To make the angular FOV scale, we coat the back surface of the doublet lens with chromium first. Then, employ laser ablation to obtain the pattern of the scale. A series of concentric circles

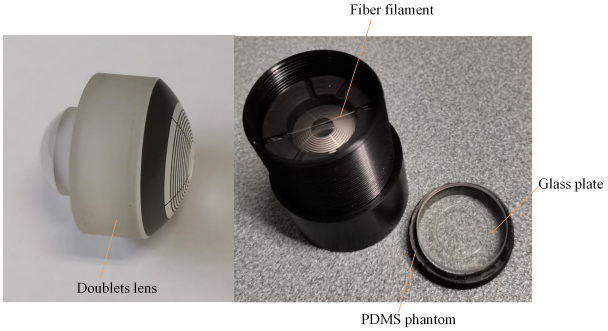


Fig. 3. The photo of the model eye tooling.

together with cross form the scale. The counts of the scale range from 24° to 60°, where the division is 4°.

The single filament which is made of optical fiber has a diameter of 0.125 mm, and it is fixed tightly 0.75 mm away from the center of the model eye. The designed distance between the small flat surface and the glass plate is 2.26 mm. The thickness of the K9 glass plate is 1 mm. The 2.5 mm thick phantom is embedded by spheres with diameters 1 $\mu$m, and the distance between each two spheres is about 40 $\mu$m. The front surface of the phantom has high flatness of the polishing level, and it sticks to the back surface of the glass plate without gap. In order to prepare the microsphere-embedded phantom, the following procedures should be going through. Firstly, drying the NIST traceable polystyrene (PS) spheres (Bangs NT15N) and mix them into curing agent (Dow Corning SYLGARD 182) homogenously with the assistance of ultrasonic water bath. Secondly, pour the mixture into pre-polymer of Polydimethylsiloxane (PDMS) and stir evenly for 1 min. The mass ratio of the curing agent the pre-polymer should be 1:10. Thirdly, pour the final mixture into a mold with polished surface. Fourthly, remove the bubbles using vacuum pump. Finally, put the mold with PDMS fluid into 70°C oven for 2h to solidify it. After demolding, a piece of solid microsphere-embedded PDMS is available for the model eye.

## 3. Experiments Results

In order to demonstrate the feasibility of using the proposed model eye, we present the experimental results. In this experiment, we employ the Van Gogh 100D of SVision Imaging working as the tested equipment.

To test the angular FOV we scan the maximum imaging area for $x$–$y$ plane by 12 mm × 12 mm.

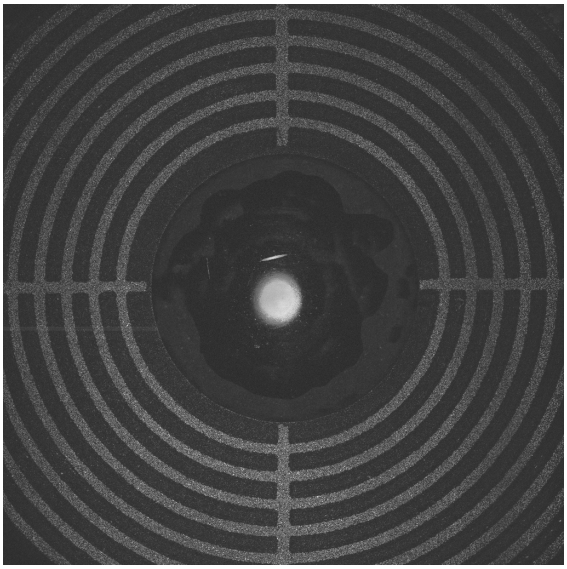

Fig. 4. The en-face image of the model eye obtained from a 3D scan.

A three-dimensional (3D) dataset is obtained, and the en-face image can be given by the OCT which is shown in Fig. 4. It can be seen that in Fig. 4, the FOV covers five rings. The smallest and the largest ring correspond to 24° and 40°, respectively. The result of the angular FOV is $(41.8° \times 41.7°) \pm 0.3°$. The nominal value of the equipment is $42° \times 42°$. The deviation of angular FOV is smaller than the tolerance of this parameter recommended by ISO 16971.

SNR falloff with scanning depth in OCT is measured here. To avoid signal saturation, we insert two neutral-density filters between the OCT and the model eye. The SNR with filters is $S_1$. The sensitivity which reflects the true SNR level of OCT system is $S_2$. The total attenuation of the filters is 26.85 dB. The total reflectivity of the model eye is −14.25 dB. Therefore, the sensitivity of the OCT can be given by $S_2(z) = S_1(z) + 26.85 + 14.25$. The model eye is put in the start position and moves along $z$-direction with a fixed pitch. The small flat surface is located at start position $z = 0.14$ mm, 10 steps are moved, and the pitch is 0.25 mm. One B-scan image can be obtained for each specific $z$-step. Find the maximum intensity for each B-scan and calculate the peak SNR $S_1(z)$ and sensitivity $S_2(z)$. Figure 5(a) shows the B-scan for $z = 0.14$ mm. Figure 5(b) presents the peak sensitivity of the OCT. The average of the peak sensitivity is 105.4 dB. As can be seen, the sensitivity of this OCT does not drop dramatically within 2.25 mm depth

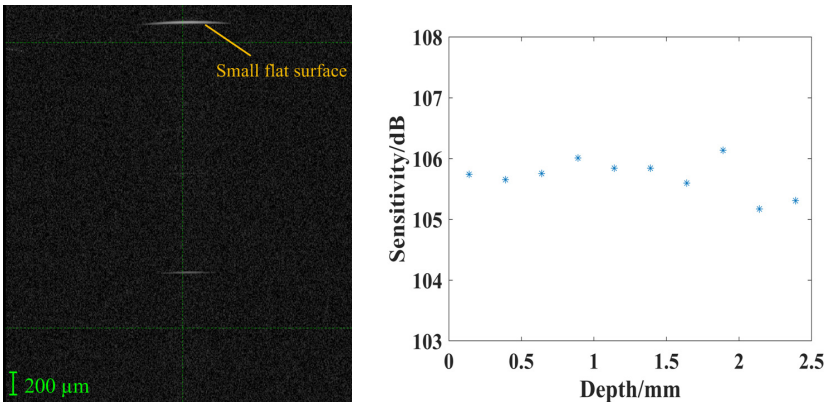


(a) (b)

Fig. 5. The SNR measurement. (a) B-scan for $z = 0.14$ mm. (b) Sensitivity for each $z$-step. The scale bar shows the optical distance.

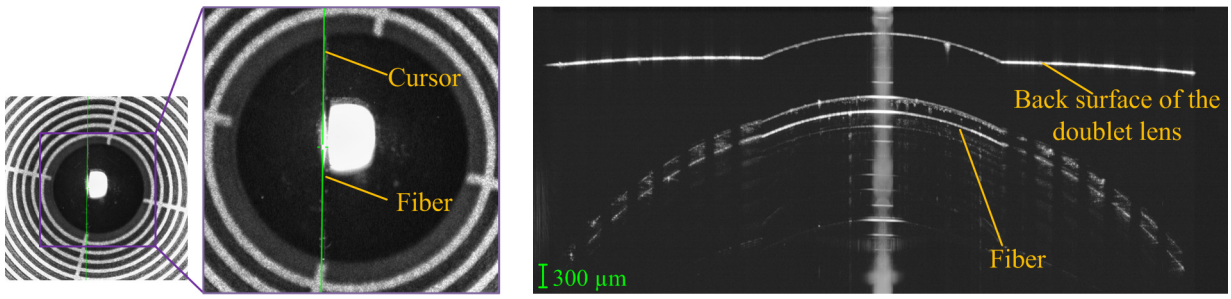


(a) (b)

Fig. 6. Co-alignment of preview and OCT scan. (a) Confocal preview image and (b) OCT B-scan. The scale bar shows the optical distance.

(depth in eye). The OCT SNR falloff can be measured using the proposed model eye.

To examine the co-alignment of the preview and the OCT scan, we use the line scan mode. The preview and the OCT scan are presented in Figs. 6(a) and 6(b). To show the transparent fiber, we present the enlarged detail in Fig. 6(a). The fiber is not right in the center of the model eye which can be improved in next mechanical design. According to Fig. 6(b), the B-scan image of the fiber is present on the full scan length; hence, the co-alignment positioning is within $\pm 125\,\mu$m. It can be seen that the line in the side part of the B-scan image is discontinuous, which results from the occlusion of the angular FOV scale. ISO 16971 recommended using a $100\,\mu$m filament (thinner than $125\,\mu$m) right in the middle of the FOV. The diameter and the centrality could be improved in future due to demanding of accurate measurement.

The depth of the empty chamber is measured via the OCT device. Place the model eye in position that equivalent to the patient eye and use the line scan mode. The preview image of the model eye is shown in Fig. 7(a), the B-scan corresponding to the arrow is presented in Fig. 7(b). The depth is 1.67 mm under the scan mode of the OCT (refractive index is 1.35), and the corresponding optical distance is 2.25 mm. The requirement of the accuracy of the depth measurement shall be better than $\pm 3\%$. Therefore, the allowable error should be smaller than 0.068 mm. The measurement error is 0.03 mm which meets the requirement.

The lateral and axial resolution can be given by imaging the micro-spheres and calculating the lateral and axial FWHMs.[8,9,16] We place the model eye in position to get strong signal of microspheres in B-scan image as shown in Fig. 8. In theory, each spot corresponds to one PS bead. As can be seen in Fig. 8, most of the PS beads in the PDMS phantom are monodispersed. Few of them stick together, and the spots are larger than others. These large spots should be eliminated in calculating the resolution. The FWHMs are calculated for the spots in each depth, and the standard deviation $\sigma$ is obtained

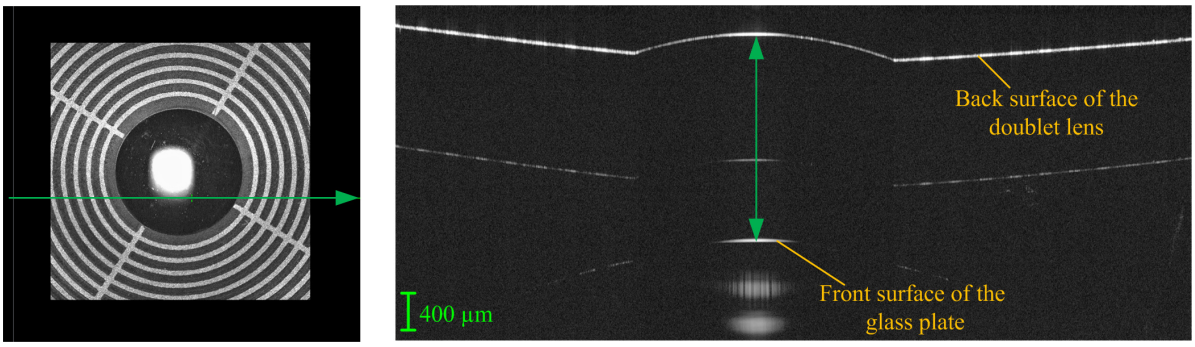


(a) (b)

Fig. 7. The depth scaling test. (a) Confocal preview image and (b) OCT B-scan. The scale bar shows the optical distance.

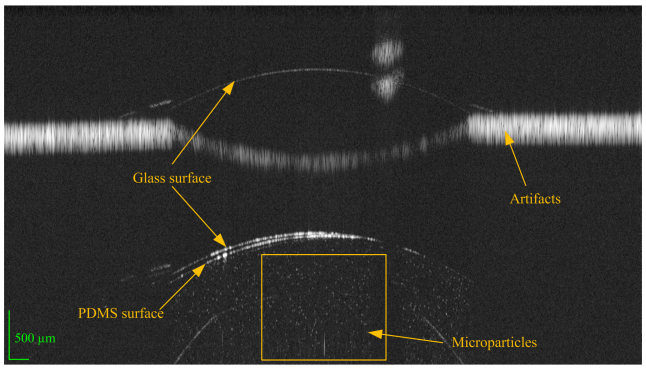


Fig. 8. B-scan image of microspheres-embedded phantom in the model eye tool. The scale bar shows the optical distance.

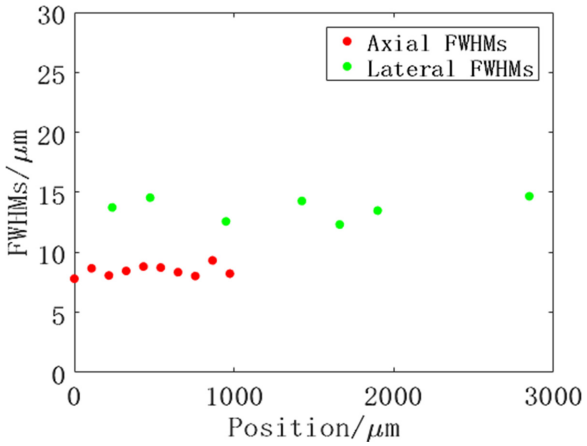


Fig. 9. The statistical result of FWHMs.

using statistical analysis. Those FWHMs larger than $\sigma$ are eliminated. The full width at half maximum (FWHM) of PSF in OCT can be given by Gaussian fitting, which can be used to value the resolution of OCT.[16] Notably, to get true FWHM the original intensity of OCT B-scan in linear domain instead of gray scale image in logarithmic domain should be used. Calculate the FWHM of PSFs for 118 valid spots within 1.082 mm × 3.164 mm area along $x$-direction and $z$-direction using Gaussian curve fitting. The statistical result is shown in Fig. 9. For the sake of concise, we show the average values of FWHMs for adjacent positions as representatives in Fig. 9. The grand average of FWHMs along $x$-direction and $z$-direction are 13.5 $\mu$m and 8.5 $\mu$m, respectively. The minimum FWHM for the two direction are 12.3 $\mu$m and 7.8 $\mu$m, respectively.

## 4. Discussion

We develop and verify the model eye tool for OCT of posterior segment in the human eye diagnosis. The ISO 16971 for the posterior segment OCT has been released with recommended calibration tool. However, the flat design of the eye ground is not suitable for the angular FOV detection. The focal plane of the lens in ISO 16971 is curved, but the angular FOV scale is straight. So, the diopter compensation should be made for all the points on the scale except the middle point. Different points on the scale need different diopter compensation values in one B-scan. However, there is only one compensation value in one B-scan of OCT imaging. Additionally, the calibration tool and methods are not given for the test of lateral resolution and SNR. Our model eye uses the same calibration method as ISO 16971 for the co-alignment of preview. ISO 16971 measures the thickness of a glass to calibrate the depth scaling which needs refractive index calibration of glass. We measure the empty room with no material in it, and no index calibration is needed. Our model eye tooling that applies the doublets lens can provide humanoid eye fundus, which benefits

the calibration of the angular FOV. The phantom with microspheres can test both the lateral and axial resolution. The small flat surface on the back surface of the doublets lens is employed to test the SNR and sensitivity of the OCT. The empty chamber between the flat surface and the glass plate is used to provide the depth scaling calibration. Avoid using glass thickness to test this parameter, our model eye is unaffected by the measurement deviation of refractive index of glass.

We present the experimental results to validate the proposed tool and demonstrate its practical use. The results indicate that the proposed tool is effective in the calibration and test of OCT for posterior segment of the human eye. Key parameters of a commercial OCT device were tested by the tool. The statistical average of corneal curvature for human eye is 8mm. So, the model eye was designed with curvature radius $R_1 = 8\,\text{mm}$ for the first lens. Parallel light coming out from the OCT can focus on the rear of the doublets. In the OCT cube scan mode, the fundus image of the model eye can be given and the angular FOV can be read directly. The measurement angular FOV of the OCT is $(41.8^\circ \times 41.7^\circ) \pm 0.3^\circ$ which is close to the nominal $42^\circ \times 42^\circ$. The SNR and sensitivity for a specific position and various depths can be given using the B-scan for the small flat surface. The average peak sensitivity 105.40 dB is obtained which demonstrates the feasibility of the SNR measurement. The co-alignment of the preview and the OCT scan is within $\pm 125\,\mu$m. The fiber is $25\,\mu$m thicker than $100\,\mu$m and not right in the middle of the eye, which could be improved in next design. Furthermore, two mutually perpendicular filaments could be used to check the co-alignment for one more direction. The measured and calibrated depth of the empty chamber are $2.25 \pm 0.004\,\text{mm}$ and $2.28 \pm 0.004\,\text{mm}$, respectively, whose difference is within the tolerance of depth scaling. So, the OCT depth imaging ability meets the parameter requirement. The model eye with microsphere-embedded phantom is imaged. The PS beads are shown in the middle (This area corresponds to the polished flat surface of the bottom in Fig. 8). There are no beads shown on the left and right sides which are caused by light blocking. The PS bead with $1\,\mu$m diameter serves as point object, whose OCT image can show PSF. The FWHM of the spots are calculated, and the OCT resolution $13.5 \pm 0.3\,\mu$m and $8.5 \pm 0.3\,\mu$m for lateral and axial direction are obtained. The measured resolutions are close to the nominal resolution $\leq 20\,\mu$m and $8\,\mu$m (in air). The artifacts are shown in Fig. 8, which is common for multi-surface object with large thickness especially industrial samples in OCT imaging. The glass surface and the PMDS surface are not perfectly superposed which does not affect the resolution measurement.

If the optical distance of each point in a $x$ scan line is the same, the line on the B-scan image is straight. The middle part of the back of the doublet lens is flat, which is cut from the sphere surface. The optical distance is the same for each point on sphere surface, and different for the flat surface. Therefore, the B-scan of the small flat surface on the back surface of the doublet lens is curved on Figs. 5(a), 6(b) and 7(b).

The proposed tool is valid for the measurement of the key parameters of OCT. The tool can be used not only in initial test of equipment performance and quality assurance, but also in certification and device licensing for retinal OCT.

## 5. Conclusions

In this study, we propose a model eye tool to emulate the human eye for the calibration of retinal OCT. The model eye can test all the key parameters of the OCT. The model eye contains a doublet lens with concentric circles on the back, a fiber filament, an empty chamber, a glass plate, and a microsphere-embedded phantom. The doublet lens is fabricated with two planoconvex lenses, which are glued together at the plane surfaces. The first spherical surface of the doublet focuses incident light onto the second spherical surface which serves as the retina surface. The concentric circles are made by laser ablation of the coating on the rear of the doublet lens, which is suitable for the angular FOV measurement. The small flat surface on the rear of the doublet is used to measure the SNR of OCT. The fiber filament can test the co-alignment of preview and the OCT scan. The empty chamber formed by the small flat surface on the rear of the doublet and the front surface of the plate is able to test the depth scaling of OCT. The PS beads in the phantom can be used to test both lateral and axial resolution. This model eye can be used as a convenient tool to evaluate and standardize the quality and accuracy of retinal OCT. In future studies, improvement will be considered to ensure more convenient operation and accurate measurement.

## Conflicts of Interest

The authors declare that there are no conflicts of interest relevant to this article.

## Acknowledgments

The study was funded by the National Key R&D Program of China (2016YFF0201005), China Post-doctoral Science Foundation (2019M660755) and Quality Infrastructure Improvement Project (ANL2001). We thank Xing Wei, Bingjie Huang, Boyang Li and Qingqing Wang from SVision Imaging, for their support during the model eye tool testing.

## References

1. D. Huang, E. A. Swanson, C. P. Lin, J. S. Schuman, W. G. Stinson, W. Chang, M. R. Hee, T. Flotte, K. Gregory, C. A. Puliafito, J. G. Fujimoto, "Optical coherence tomography," *Science* **254**, 1178–1181 (1991).
2. X. Wang, Z. Li, N. Nan, Y. Bu, A. Zeng, S. Osami, X. Wang, "A simple system of swept source optical coherence tomography for a large imaging depth range," *Opt. Commun.* **431**, S003040181830779X-(2018).
3. J. A. Izatt, M. R. Hee, E. A. Swanson, C. P. Lin, D. Huang, J. S. Schuman, C. A. Puliafito, J. G. Fujimoto, "Micrometer-scale resolution imaging of the anterior eye in vivo with optical coherence tomography," *Arch. Ophthalmol.* **112**(12), 1584–1589 (1994).
4. G. N. Girish, T. Bibhash, R. C. Sohini, R. K. Abhishek, R. Jeny, "Segmentation of intra-retinal cysts from optical coherence tomography images using a fully convolutional neural network model," *IEEE J. Biomed. Health Inform.* **23**(1), 296–304 (2019).
5. X. Zou, G. Tan, Y. Shao, "Application of optical coherence tomography angiography in ocular anterior segment diseases," *Chin. J. Exp. Ophthalmol.* **36**(5), 398–400 (2018).
6. P. D. Woolliams, P. H. Tomlins, "Estimating the resolution of a commercial optical coherence tomography system with limited spatial sampling," *Meas. Sci. Technol.* **22**(6), 065502 (2011).
7. R. C. Chang, Robert, P. Johnson, C. M. Stafford, J. Hwang, "Fabrication and characterization of a multilayered optical tissue model with embedded scattering microspheres in polymeric materials," *Biomed. Opt. Express* **3**(6), 1326–1339 (2012).
8. A. Agrawal, T. J. Pfefer, N. Gilani, R. Drezek, "Three-dimensional characterization of optical coherence tomography point spread functions with a nanoparticle-embedded phantom," *Opt. Lett.* **35**(13), 2269–2271 (2010).
9. P. H. Tomlins, R. A. Ferguson, C. Hart, P. D. Woolliams, "Point-spread function phantoms for optical coherence tomography," National Physical Laboratory (2009).
10. Z. Hu, B. Hao, W. Liu, B. Hong, "Research on point spread function phantom fabrication and application for evaluating resolution performance of OCT systems," *Acta Opt. Sin.* **35**(4), 0417001 (2015).
11. Z. Hu, W. Liu, B. Hong, B. Hao, L. Wang, J. Li, "A physical model eye with 3D resolution test targets for optical coherence tomography," *Opto-Electron. Eng.* **41**(12), 28–38 (2014).
12. Z. Cao, Z. Ding, Z. Hu, W. Qiao, W. Liu, X. Chen, "Model eyes with curved multilayer structure for the axial resolution evaluation of an ophthalmic optical coherence tomography device," *J. Innov. Opt. Health Sci.* **11**(2), 1850013 (2018).
13. J. Baxi, W. Calhoun, Y. J. Sepah, D. X. Hammer, A. Agrawal, "Retina-simulating phantom for optical coherence tomography," *J. Biomed. Opt.* **19**(2), 21106 (2014).
14. H. J. Lee, N. M. Samiudin, T. G. Lee, I. Doh, S. W. Lee, "Retina phantom for the evaluation of optical coherence tomography angiography based on microfluidic channels," *Biomed. Opt. Express* **10**(11), 5535 (2019).
15. ISO/TC 172/SC 7, "Ophthalmic instruments — Optical coherence tomography for the posterior segment of the human eye," Switzerland (2015).
16. A. Fouad, T. J. Pfefer, C. Chen, W. Gong, A. Agrawal, P. H. Tomlins, P. D. Woolliams, R. A. Drezek, Y. Chen, "Variations in optical coherence tomography resolution and uniformity: A multi-system performance comparison," *Biomed. Opt. Express* **5**(7), 2066–2081 (2014).